CHAPTER 8

ECG-Derived Respiratory Frequency Estimation

Raquel Bailón, Leif Sörnmo, and Pablo Laguna

8.1 Introduction

The respiratory signal is usually recorded with techniques like spirometry, pneumography, or plethysmography. These techniques require the use of cumbersome devices that may interfere with natural breathing, and which are unmanageable in certain applications such as ambulatory monitoring, stress testing, and sleep studies. Nonetheless, the joint study of the respiratory and cardiac systems is of great interest in these applications and the use of methods for indirect extraction of respiratory information is particularly attractive to pursue. One example of application would be the analysis of the influence of the respiratory system in heart rate variability (HRV) during stress testing, since it has been observed that the power in the very high frequency band (from 0.4 Hz to half the mean heart rate expressed in Hz) exhibits potential value in coronary artery disease diagnosis [1], and HRV power spectrum is dependent on respiratory frequency. Another field of application would be sleep studies, since the diagnosis of apnea could be based on fewer and simpler measurements, like the ECG, rather than on the polysomnogram, which is expensive to record.

It is well known that the respiratory activity influences electrocardiographic measurements in various ways. During the respiratory cycle, chest movements and changes in the thorax impedance distribution due to filling and emptying of the lungs cause a rotation of the electrical axis of the heart which affects beat morphology. The effect of respiration-induced heart displacement on the ECG was first studied by Einthoven et al. [2] and quantified in further detail in [3, 4]. It has been experimentally shown that "electrical rotation" during the respiratory cycle is mainly caused by the motion of the electrodes relative to the heart, and that thoracic impedance variations contribute to the electrical rotation just as a second-order effect [5].

Furthermore, it is well known that respiration modulates heart rate such that it increases during inspiration and decreases during expiration [6, 7]. It has also been shown that the mechanical action of respiration results in the same kind of frequency content in the ECG spectrum as does HRV [8].

Figure 8.1 displays an ECG lead as well as the related heart rate (HR) and respiratory signals in which the ECG amplitude is modulated with a frequency similar to that of the respiratory signal. It seems that the ECG amplitude modulation is not in phase with the respiratory signal. It can also be seen that the HR and the

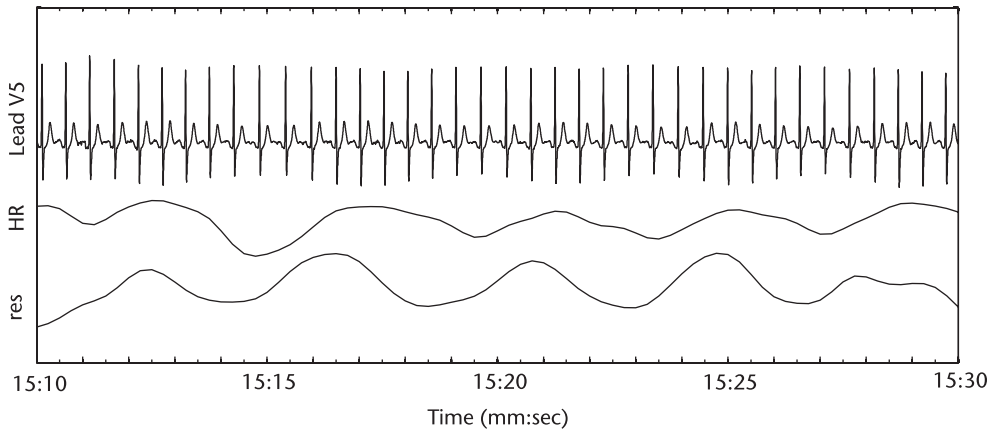

Figure 8.1 Simultaneous ECG lead V5 (top), HR (middle), and respiration (bottom) signals.

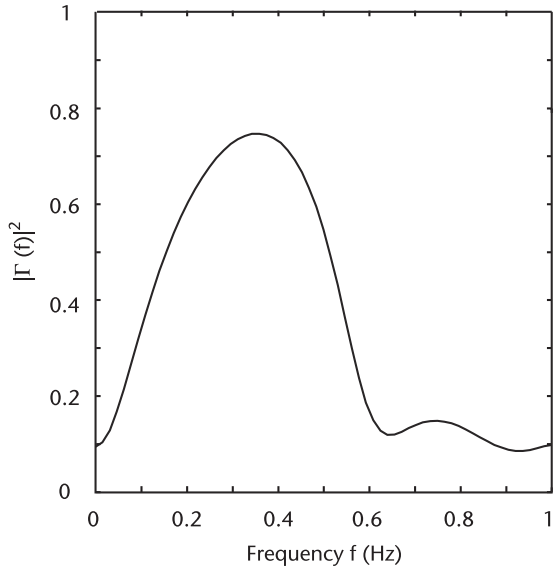

Figure 8.2 Magnitude squared coherence $|\Gamma(f)|^2$ between HR and respiratory signals of Figure 8.1. The largest value of $|\Gamma(f)|^2$ is located around 0.3 Hz.

respiratory signal fluctuate at a similar frequency. Figure 8.2 displays the magnitude squared coherence between HR and respiratory signal. The magnitude squared coherence is defined as being a measure of the correlation between two signals at a given frequency [9]. It can be seen that the largest value is located around 0.3 Hz, meaning that the signals are strongly correlated at this frequency.

Several studies have developed signal processing techniques to extract respiratory information from the ECG, so-called ECG-derived respiratory (EDR) information. Some techniques are based on respiration-induced variations in beat-to-beat morphology [5, 10–24], while others attempt to extract respiratory information from the HR [25–27].

The first EDR method based on morphologic variations dates back to 1974 when Wang and Calvert [10] proposed a model for the mechanics of the heart with

respect to respired air volume of the lungs, and a technique for monitoring respiratory rate and depth using the vectorcardiogram (VCG). Later, Pinciroli et al. [11] and Moody et al. [5] proposed algorithms which exploit variations in the direction of the heart's electrical axis. Recently, the respiratory frequency was obtained as the dominant frequency of the estimated rotation angles of the electrical axis [22]; this method was later extended to handle noisy exercise ECGs [28]. Variations in the inertial axes and center of gravity of QRS-VCG loops were also used to estimate the respiratory signal [23]. For single-lead recordings, amplitude modulation of ECG waves has been used to derive a respiratory signal, especially in the context of sleep apnea studies [14, 18, 24]. Yet another approach to the EDR problem has been to apply a bandpass filter to the single-lead ECG, selecting the usual respiratory frequency band from 0.2 to 0.4 Hz [20].

Some methods derive respiratory information solely from the HR series. The respiratory frequency was estimated from the RR interval series using singular value decomposition (SVD) to track the most important instantaneous frequencies of the interval series [25]. Some years later, the respiratory frequency present in the HR series was derived using the S-transform [26]. Respiratory frequency patterns were derived from the RR interval series using autoregressive (AR) model-based methods in stationary [29] and nonstationary situations [27].

There are also some methods which derive the respiratory signal using both beat morphology and HR information. The cross-power spectrum of the EDR signals obtained from morphologic variations and HR was used to enhance the respiratory frequency [22]. Another approach was to use an adaptive filter so as to enhance the respiration-related common component present in the EDR signals derived from beat morphology and HR [30].

In this chapter the estimation of respiratory frequency from the ECG will be addressed. Algorithms deriving a respiratory signal from the ECG, so-called EDR algorithms, are presented, as well as the signal preprocessing needed for their proper performance. Electrocardiogram-derived respiration algorithms may be divided into three categories: Section 8.2 presents EDR algorithms based on beat-to-beat morphologic variations (which can be applied to single- or multilead ECGs), Section 8.3 describes EDR algorithms based on HR information, and Section 8.4 describes EDR algorithms using both beat morphology and HR information. One of the main interests in deriving the EDR signal is the estimation of respiratory frequency. Therefore, spectral analysis of the previously derived EDR signals is described in Section 8.5 and related estimation of the respiratory frequency. The general procedure to estimate the respiratory frequency from the ECG is summarized in Figure 8.3.

In order to evaluate and compare the performance of the EDR algorithms, the derived respiratory information should be compared to respiratory information simultaneously recorded. Performance measurements may vary depending on the particular goal for which the EDR algorithm is applied. For example, the respiratory frequency estimated from the ECG can be compared to that estimated from a simultaneously recorded respiratory signal, considered as gold standard [28]. When simultaneous recordings of ECG and respiratory signal are unavailable, an alternative is the design of a simulation study, where all signal parameters can be controlled and compared to the derived ones. This approach is described in Section 8.6.

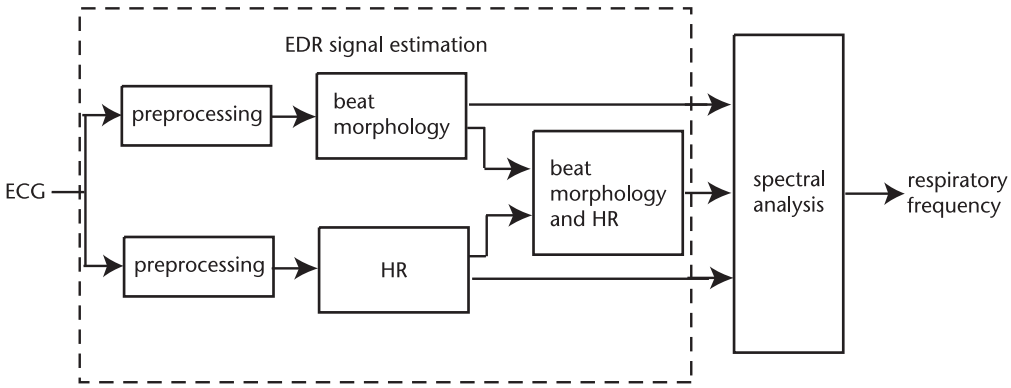

Figure 8.3 Block diagram of the estimation of the respiratory frequency from the ECG.

8.2 EDR Algorithms Based on Beat Morphology

Several methods have been proposed to derive the respiratory signal from the ECG using beat-to-beat morphologic variations. The underlying idea behind these methods is that the electrical axis of the heart changes its direction during the respiratory cycle due to motion of the electrodes relative to the heart and heterogeneous variations in the thorax impedance caused by the filling and emptying of the lungs. Therefore, the EDR signal may be estimated from the fluctuations of the heart's electrical axis. The way to estimate variations in axis direction is what mainly differs from one method to another.

In this section, three different types of EDR algorithms based on beat morphology are described, namely those based on wave amplitudes (Section 8.2.1), the multilead QRS area (Section 8.2.2) and the QRS-VCG loop alignment (Section 8.2.3). Amplitude EDR algorithms can be applied to single-lead ECGs while the multilead QRS area and the QRS-VCG loop alignment methods require at least two orthogonal leads.

Adequate performance of an EDR algorithm requires certain types of preprocessing of the raw ECG. First of all, QRS complexes must be detected and clustered based on their morphology, since only beats with the dominant morphology should be analyzed. The dominant morphology is the one corresponding to the largest class, whose beats typically originate from the sinoatrial node. Baseline wander should be attenuated in order not to introduce a rotation of the electrical axis unrelated to respiration. Certain EDR algorithms, like the QRS-VCG loop alignment, require VCG signals which, if unavailable, may have to be synthesized from the standard 12-lead ECG by means of the inverse Dower transformation [31]; see Appendix 8A for further details.

Additional preprocessing has been proposed to make the EDR algorithm robust when processing noisy ECGs such as those recorded during exercise [28]. Noisy beats can be substituted on a lead-by-lead basis using an exponentially updated average beat. The idea is that excessive noise present in a single lead would mask the rotation information present in the remaining leads. In such cases, the noisy beat is substituted so that the rotation information of the remaining leads is preserved.

Two different kinds of noise are common in ECGs: high-frequency (HF) noise mainly due to muscle activity, and low-frequency (LF) noise due to remaining baseline wander unattenuated by the preprocessing step. Consequently, a high frequency SNR, SNR_{HF}, and a low-frequency SNR, SNR_{LF}, can be defined to determine beats for substitution. The SNR_{HF} is defined as the ratio of the peak-to-peak amplitude in an interval centered around the QRS mark, and the root-mean-square (RMS) value of the HF noise in an HR-dependent interval following the QRS mark to avoid QRS mediated HF components. The SNR_{LF} is defined as the ratio of the peak-to-peak amplitude of the exponentially updated average beat and the RMS value of the residual ECG after average beat substraction and lowpass filtering computed over the whole beat interval. Figure 8.4 displays an example of a noisy beat, the exponentially updated average beat, the HF noise resulting from highpass filtering the noisy beat with a cutoff frequency of 20 Hz, and the residual ECG after average beat substraction and lowpass filtering with a cutoff frequency of 20 Hz. Beats whose SNR_{HF} is below a threshold, η_{HF}, or whose SNR_{LF} is below another threshold, η_{LF}, are substituted by their corresponding averaged beats. Figure 8.5 displays a VCG before and after substitution of noisy beats, as well as the estimated EDR signals and related respiratory signal. The spectra obtained from the EDR signals and the respiratory signal of Figure 8.5 are displayed in Figure 8.6. The substitution of noisy beats improves the estimation of the respiratory frequency since the largest

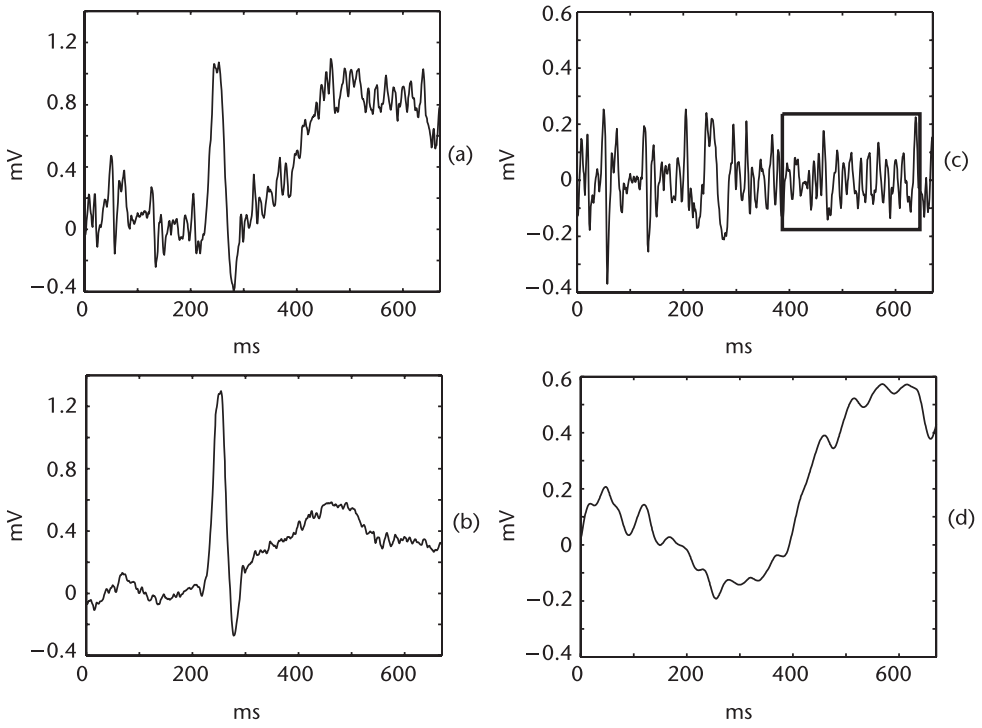

Figure 8.4 An example of (a) a noisy beat, (b) the exponentially updated average beat, (c) the HF noise resulting from highpass filtering the noisy beat with a cutoff frequency of 20 Hz (the interval over which the RMS is computed has been marked with a box), and (d) the residual ECG after average beat substraction and lowpass filtering with a cutoff frequency of 20 Hz.

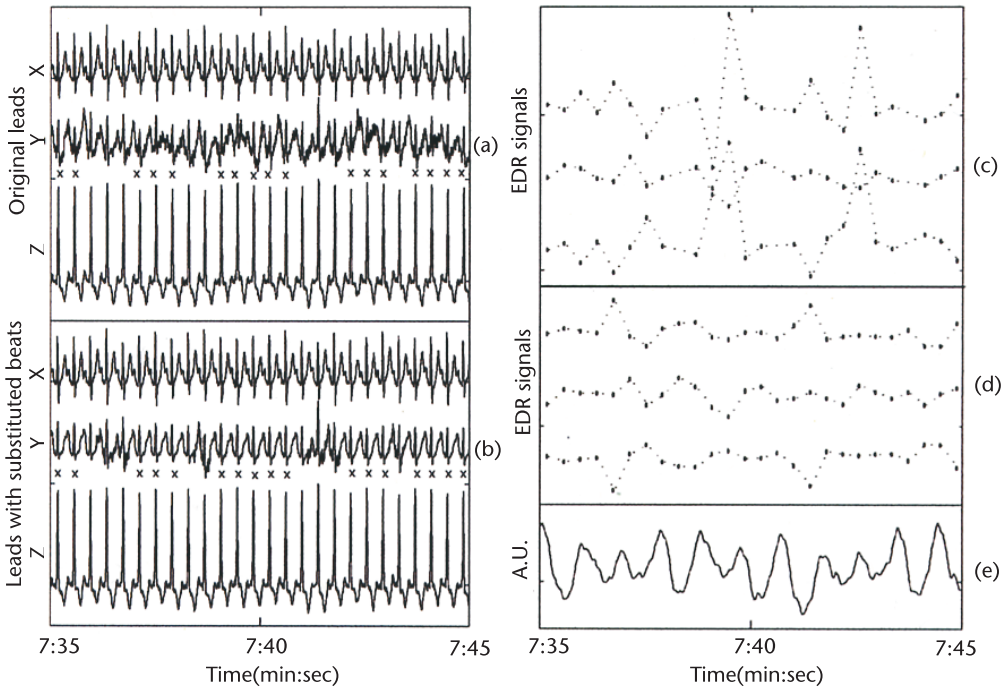

Figure 8.5 The VCG leads (a) before and (b) after substitution of noisy beats. The EDR signals (linear interpolation points have been used) estimated (c) before and (d) after substitution of noisy beats, and (e) the related respiratory signal. Recordings were taken during a stress test. Substituted beats in lead Y have been marked (×). The following parameter values are used: $\eta_{HF} = 20$ and $\eta_{LF} = 3$.

peak of the EDR spectrum has been shifted such that it coincides with the largest peak of the respiratory spectrum.

8.2.1 Amplitude EDR Algorithms

When only single-lead ECGs are available, amplitude modulation of the ECG waves has been used to derive a respiratory signal, especially in the context of sleep apnea studies. For example, the sum of the absolute R and S wave amplitudes is used as a respiratory estimate in the detection of apneic events in infants [14]. Two methods for deriving an EDR signal from single-lead ECG amplitudes have been compared [18]: The amplitude of the R wave is measured either with respect to the baseline or differentially with respect to the amplitude of the S wave for each QRS complex. Both EDR signals are used to detect breaths using a peak detection algorithm; the EDR signal based on the differential measure of the R wave amplitude with respect to the S wave amplitude obtained higher sensitivity (77% compared to 68%) and positive predictivity (56% compared to 49%).

Alternatively, an EDR signal can be obtained from single-lead ECGs by calculating the area enclosed by the baseline-corrected ECG within a fixed interval of the QRS complex. The area measurements have been found to be more stable and less prone to noise than amplitude measurements [5]. Such an EDR signal has been used in the detection of obstructive sleep apnea [21, 32]. The error between respiratory

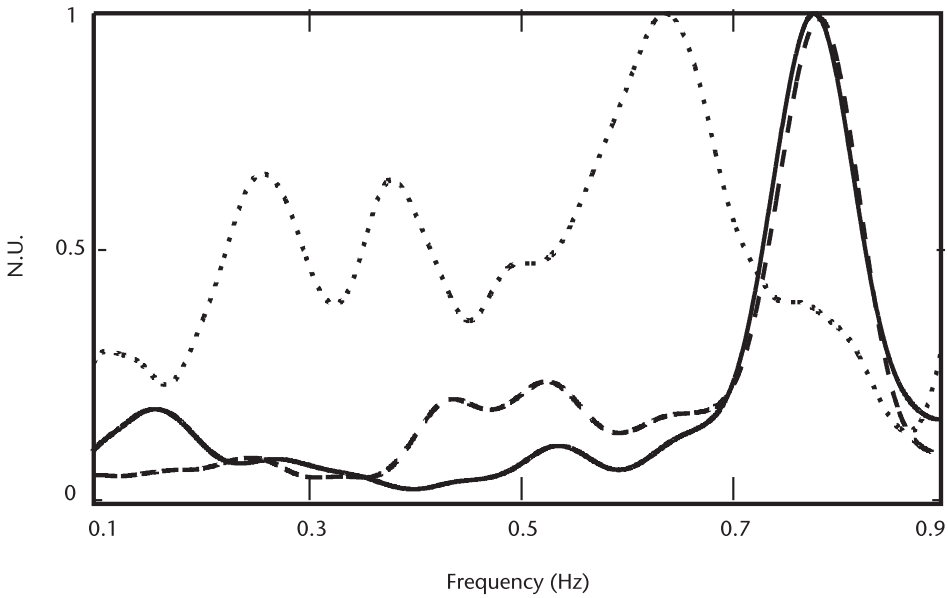

Figure 8.6 Power spectrum of the respiratory signal (solid line), and the EDR signals before (dotted line) and after (dashed line) substitution of noisy beats in normalized units (N.U.).

rate extracted from such an EDR signal and from a simultaneous airflow signal was reported to be −0.3 breaths per minute (−0.005 Hz) [32].

An EDR signal can also be obtained from the T wave rather than from the QRS complex: the signal segment following each QRS complex is linearly detrended and its average absolute value can be used as a sample of an EDR signal [17].

A different approach to the EDR problem is to filter the single-lead ECG with a passband corresponding to the usual respiratory frequency band. For example, the discrete wavelet transform has been applied to the single-lead ECG and the scale corresponding to the frequency band 0.2 to 0.4 Hz can be selected as an EDR signal [20]. Correlation coefficients between respiratory frequency extracted from the EDR signal and from simultaneous airflow signal exceeding 0.9 were reported.

Due to the thorax anisotropy and its intersubject variability together with the intersubject electrical axis variability, respiration may have a different effect on different ECG leads, implying that the lead most influenced by respiration often changes from subject to subject [33]. Single-lead EDR algorithms are reported to work better if the lead axis is significantly different from the mean electrical axis since a relatively larger EDR signal results in such cases. It has been experimentally shown that respiration-related ECG changes are reflected primarily in the direction (affected mainly by motion of the electrodes relative to the heart) and not in the magnitude (affected mainly by thoracic impedance variations) of the mean electrical axis; therefore, a lead perpendicular to the mean electrical axis would produce a larger EDR signal than a parallel lead [5]. Principal component analysis may be applied to the 12-lead ECG in order to obtain a virtual lead, linear combination of the original ones, most influenced by respiration [32].

8.2.2 Multilead QRS Area EDR Algorithm

In this method, the projection of the mean electrical axis on the plane defined by two leads is considered. The variation in angle between this projection and a reference lead is used as an estimate of the EDR signal [5]. The area of the ith QRS complex, occurring at time instant t_i, is computed over a fixed time interval in each lead, thus being proportional to the projection of the mean electrical axis on that lead. Consider the projection of the mean electrical axis on the plane jk, defined by orthogonal leads j and k, at time instant t_i, which is denoted as the vector $\overline{\mathbf{m}}(t_i)$,

$$\overline{\mathbf{m}}(t_i) = \begin{bmatrix} \dfrac{1}{\delta_2+\delta_1}\displaystyle\int_{t_i-\delta_1}^{t_i+\delta_2} \|\mathbf{m}(t)\|_2 \cos(\theta_{jk}(t))dt \\ \dfrac{1}{\delta_2+\delta_1}\displaystyle\int_{t_i-\delta_1}^{t_i+\delta_2} \|\mathbf{m}(t)\|_2 \sin(\theta_{jk}(t))dt \end{bmatrix} = \frac{1}{\delta_2+\delta_1}\begin{bmatrix} A_j(t_i) \\ A_k(t_i) \end{bmatrix} \tag{8.1}$$

where $\mathbf{m}(t)$ is the instantaneous projection of the electrical axis on the plane jk, $\theta_{jk}(t)$ is the angle between $\mathbf{m}(t)$ and lead j, $A_j(t_i)$ represents the QRS area in lead j, δ_1 and δ_2 define the integration interval over which the mean is computed, and the operator $\|.\|_2$ denotes the Euclidean distance. The term $\|\mathbf{m}(t)\|_2 \cos(\theta_{jk}(t))$ represents the projection of $\mathbf{m}(t)$ on lead j, and $\|\mathbf{m}(t)\|_2 \sin(\theta_{jk}(t))$ the projection of $\mathbf{m}(t)$ on lead k. The projection angle of the mean electrical axis on the plane jk with respect to lead j, $\overline{\theta}_{jk}(t_i)$, can be estimated as

$$\overline{\theta}_{jk}(t_i) = \arctan(A_k(t_i)/A_j(t_i)) \tag{8.2}$$

See Figure 8.7. Finally, the fluctuations of the $\overline{\theta}_{jk}(t_i)$ series are used as an EDR signal. The values of δ_1 and δ_2 depend on the application; they can be chosen so as to comprise the whole QRS complex, a symmetric window around the QRS fiducial point, or an asymmetric window in order to reduce the QRS morphologic variations unrelated to respiration but related to other conditions such as exercise. Figure 8.8 displays an example of the multilead QRS area EDR algorithm, where the angle series $\overline{\theta}_{YZ}(t_i)$ can be seen as well as the two orthogonal VCG leads Y and Z and the related respiratory signal.

The multilead QRS area EDR algorithm has been further studied [13] and applied in HRV analysis [12], sleep studies [19], and used for ambulatory monitoring [16].

Using a similar principle, the areas of the QRS complexes in eight leads have been used to define an EDR signal [15]. First, an eight-dimensional space is defined by eigenvalue analysis of a learning set; then, each eight-dimensional QRS area vector is projected onto the main direction, which is considered as particularly sensitive to respiratory information, and then used as an EDR signal.

A different approach has been addressed to estimate the direction of the projection of the mean electrical axis on the plane defined by two orthogonal leads. The least-squares (LS) straight line is computed which fits the projection of the VCG

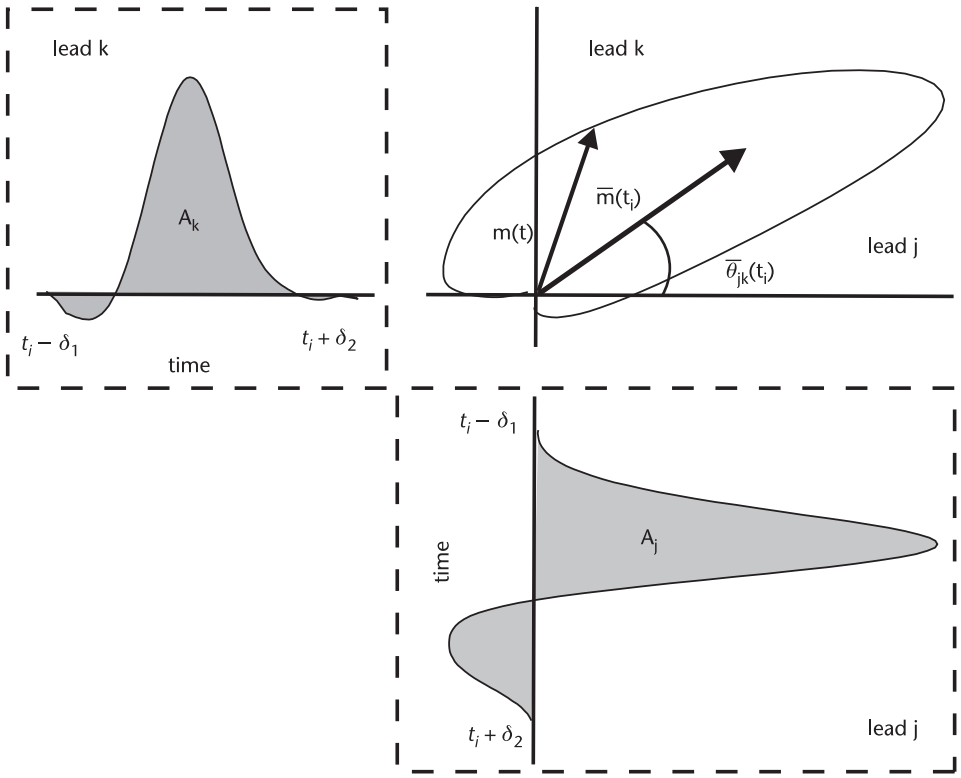

Figure 8.7 Illustration of the mean heart's electrical axis projected on the plane jk.

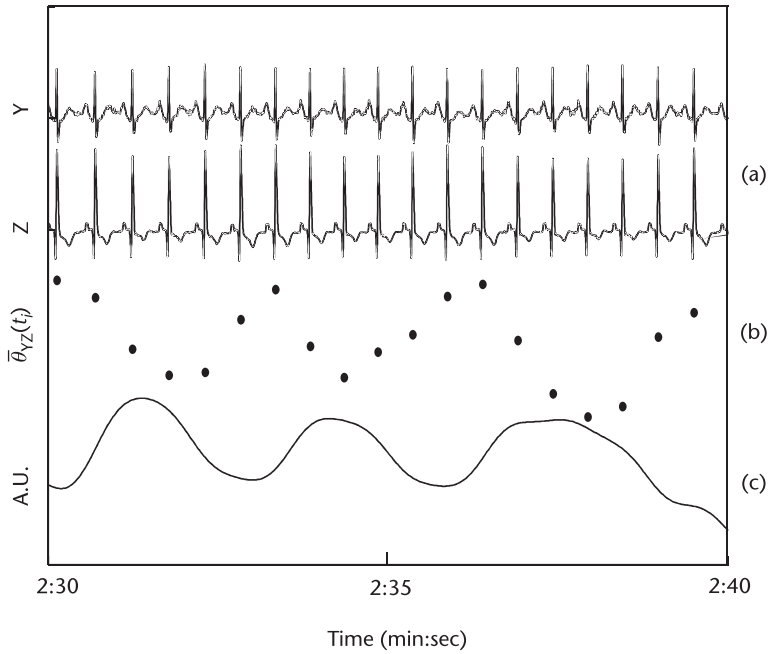

Figure 8.8 Multilead QRS area EDR algorithm: (a) leads Y and Z, (b) the estimated EDR signal $\overline{\theta}_{YZ}(t_i)$, and (c) the related respiratory signal. Recordings were taken during a stress test. The parameter values used are: $\delta_1 = 60$ ms, $\delta_2 = 20$ ms.

on the plane defined by two leads. Then, the variations of the angle that forms the LS fit with a reference direction constitutes the EDR signal [11]. It has been stated that angles obtained from different pairs of orthogonal leads cannot be expected to provide the same range of amplitude variation. Furthermore, the lead configuration yielding the EDR signal with largest amplitude variation often changes from subject to subject [33].

8.2.3 QRS-VCG Loop Alignment EDR Algorithm

This method is based on LS estimation of the rotation angles of the electrical axis around the three-dimensional orthogonal axes between successive VCG loops and a reference loop [22]. At each time instant t_i, the method performs minimization of a normalized distance ε between a reference loop ($N\times 3$ matrix $\mathbf{Y_R}$, where the columns contain the QRS complex of the X, Y, and Z leads) and each observed loop (($N+2\Delta)\times 3$ matrix $\mathbf{Y}$), with respect to rotation (3×3 matrix $\mathbf{Q}$), amplitude scaling (scalar γ), and time synchronization ($N\times(N+2\Delta)$ matrix $\mathbf{J}_\tau$) [34, 35]:

$$\varepsilon_{min} = \min_{\gamma,\tau,\mathbf{Q}}(\varepsilon) = \min_{\gamma,\tau,\mathbf{Q}} \frac{\|\mathbf{Y_R} - \gamma\mathbf{J}_\tau\mathbf{Y}\mathbf{Q}\|_F^2}{\|\gamma\mathbf{J}_\tau\mathbf{Y}\mathbf{Q}\|_F^2} \tag{8.3}$$

where

$$\mathbf{J}_\tau = [\,\mathbf{0}_{\Delta-\tau}\ \mathbf{I}\ \mathbf{0}_{\Delta+\tau}\,] \tag{8.4}$$

and N is the number of samples of the QRS complex analysis window. The parameter Δ denotes the number of symmetrically augmented samples which allow for time synchronization with $\tau = -\Delta, \ldots, \Delta$. The dimensions of the $\mathbf{0}_{\Delta-\tau}$, $\mathbf{0}_{\Delta+\tau}$, and $\mathbf{I}$ (identity) matrices are $N\times(\Delta-\tau)$, $N\times(\Delta+\tau)$, and $N\times N$, respectively. The operator $\|\cdot\|_F^2$ denotes the Frobenius norm. For simplicity, the dependence on time instant t_i is omitted in the notation [i.e., $\varepsilon = \varepsilon(t_i)$, $\mathbf{Y_R} = \mathbf{Y_R}(t_i)$, $\mathbf{Y} = \mathbf{Y}(t_i)$, $\mathbf{Q} = \mathbf{Q}(t_i)$, and $\gamma = \gamma(t_i)$].

The rotation matrix $\mathbf{Q}$ can be viewed as three successive rotations around each axis (lead), defined by the rotation angles ϕ_X, ϕ_Y, and ϕ_Z,

$$\begin{aligned}\mathbf{Q} &= \begin{bmatrix} 1 & 0 & 0 \\ 0 & \cos(\phi_X) & \sin(\phi_X) \\ 0 & -\sin(\phi_X) & \cos(\phi_X) \end{bmatrix} \begin{bmatrix} \cos(\phi_Y) & 0 & \sin(\phi_Y) \\ 0 & 1 & 0 \\ -\sin(\phi_Y) & 0 & \cos(\phi_Y) \end{bmatrix} \begin{bmatrix} \cos(\phi_Z) & \sin(\phi_Z) & 0 \\ -\sin(\phi_Z) & \cos(\phi_Z) & 0 \\ 0 & 0 & 1 \end{bmatrix} \\ &= \begin{bmatrix} * & \sin(\phi_Z)\cos(\phi_Y) & \sin(\phi_Y) \\ * & * & \sin(\phi_X)\cos(\phi_Y) \\ * & * & * \end{bmatrix}\end{aligned} \tag{8.5}$$

where the asterisk $*$ denotes an omitted matrix entry.

The normalized distance ε is minimized by first finding estimates of γ and $\mathbf{Q}$ for every value of τ and then selecting that τ for which ε is minimum. For a fixed value of τ, the optimal estimator of $\mathbf{Q}$ is given by [34]

$$\hat{\mathbf{Q}}_\tau = \mathbf{V}_\tau\mathbf{U}_\tau^T \tag{8.6}$$

where the matrices $\mathbf{U}_\tau$ and $\mathbf{V}_\tau$ contain the left and right singular vectors from the SVD of $\mathbf{Z}_\tau = \mathbf{Y}_\mathbf{R}^T \mathbf{J}_\tau \mathbf{Y}$. The estimate of γ is then obtained by [35]

$$\hat{\gamma}_\tau = \frac{tr(\mathbf{Y_R}^T \mathbf{Y_R})}{tr(\mathbf{Y_R}^T \mathbf{J}_\tau^T \mathbf{Y} \hat{\mathbf{Q}}_\tau)} \tag{8.7}$$

The parameters $\hat{\mathbf{Q}}_\tau$ and $\hat{\gamma}_\tau$ are calculated for all values of τ, with $\hat{\mathbf{Q}}$ resulting from that τ which yields the minimal error ε. Finally, the rotation angles are estimated from $\hat{\mathbf{Q}}$ using the structure in (8.5) [22],

$$\hat{\phi}_Y = \arcsin(\hat{q}_{13}) \tag{8.8}$$

$$\hat{\phi}_X = \arcsin\left(\frac{\hat{q}_{23}}{\cos(\hat{\phi}_Y)}\right) \tag{8.9}$$

$$\hat{\phi}_Z = \arcsin\left(\frac{\hat{q}_{12}}{\cos(\hat{\phi}_Y)}\right) \tag{8.10}$$

where the estimate $\hat{q}_{kl}$ denotes the (k,l) entry of $\hat{\mathbf{Q}}$.

In certain situations, such as during ischemia, QRS morphology exhibits long-term variations unrelated to respiration. This motivates a continuous update of the reference loop in order to avoid the estimation of rotation angles generated by such variations rather than by respiration [28]. The reference loop is exponentially updated as

$$\mathbf{Y_R}(i+1) = \alpha \mathbf{Y_R}(i) + (1-\alpha)\mathbf{Y}(i+1) \tag{8.11}$$

where i denotes the beat index at time instant t_i [i.e., $\mathbf{Y_R}(t_i) = \mathbf{Y_R}(i)$ and $\mathbf{Y}(t_i) = \mathbf{Y}(i)$]. The parameter α is chosen such that long-term morphologic variations are tracked while adaptation to noise and short-term respiratory variations is avoided. The initial reference loop $\mathbf{Y_R}(1)$ can be defined as the average of the first loops in order to obtain a reliable reference. Figure 8.9 displays lead X of $\mathbf{Y_R}$ at the beginning and peak exercise of a stress test, and illustrates the extent by which QRS morphology may change during exercise.

An example of the method's performance is presented in Figure 8.10 where the estimated rotation angle series are displayed as well as the VCG leads and the related respiratory signal.

Unreliable angle estimates may be observed at poor SNRs or in the presence of ectopic beats, calling for an approach which makes the algorithm robust against outlier estimates [28]. Such estimates are detected when the absolute value of the angle estimates exceed a lead-dependent threshold $\eta_j(t_i)$ ($j \in \{X, Y, Z\}$). The threshold $\eta_j(t_i)$ is defined as the running standard deviation (SD) of the N_e most recent angle estimates, multiplied by a factor C. For $i < N_e$, $\eta_j(t_i)$ is computed from the available estimates. Outliers are replaced by the angle estimates obtained by reperforming the minimization in (8.3), but excluding the value of τ which produced the outlier estimate. The new estimates are only accepted if they do not exceed the threshold $\eta_j(t_i)$; if no acceptable value of τ is found, the EDR signal contains a gap and the reference loop $\mathbf{Y_R}$ in (8.11) is not updated. This procedure is illustrated by Figure 8.11.

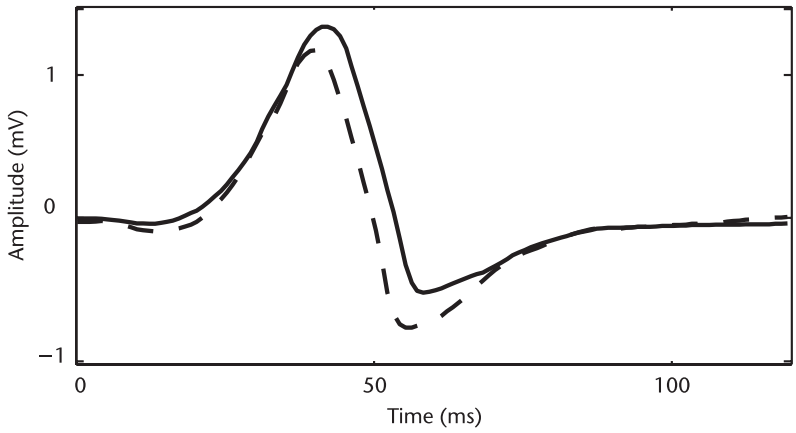

Figure 8.9 The reference loop $\mathbf{Y_R}$ (lead X) at onset (solid line) and peak exercise (dashed line) of a stress test.

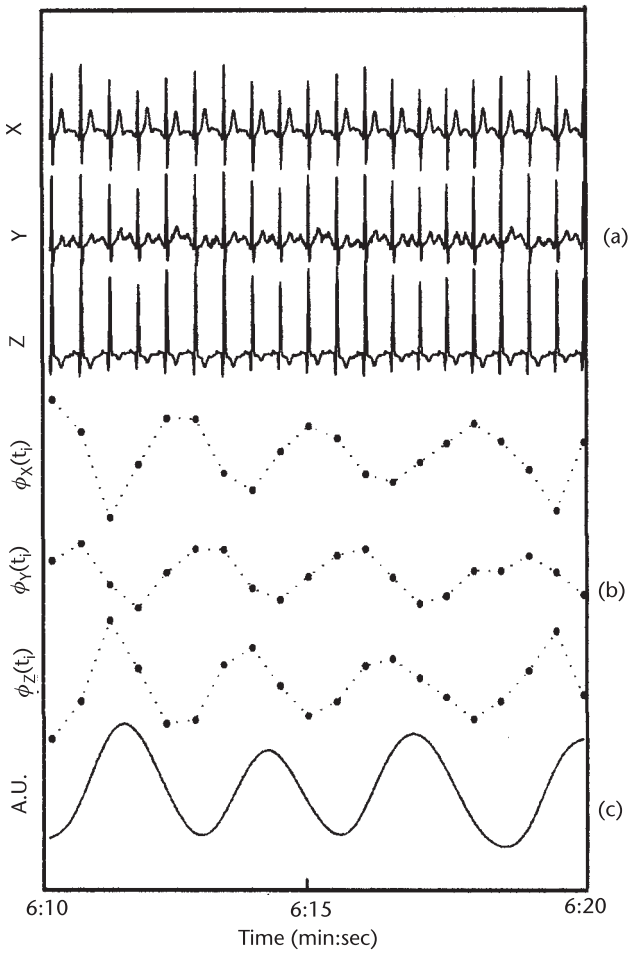

Figure 8.10 QRS-VCG loop alignment EDR algorithm: (a) the VCG leads, (b) the estimated EDR signals (linear interpolation points have been used), and (c) the related respiratory signal. Recordings were taken during a stress test. The following parameter values are used: $N = 120$ ms, $\Delta = 30$ ms in steps of 1 ms, and $\alpha = 0.8$.

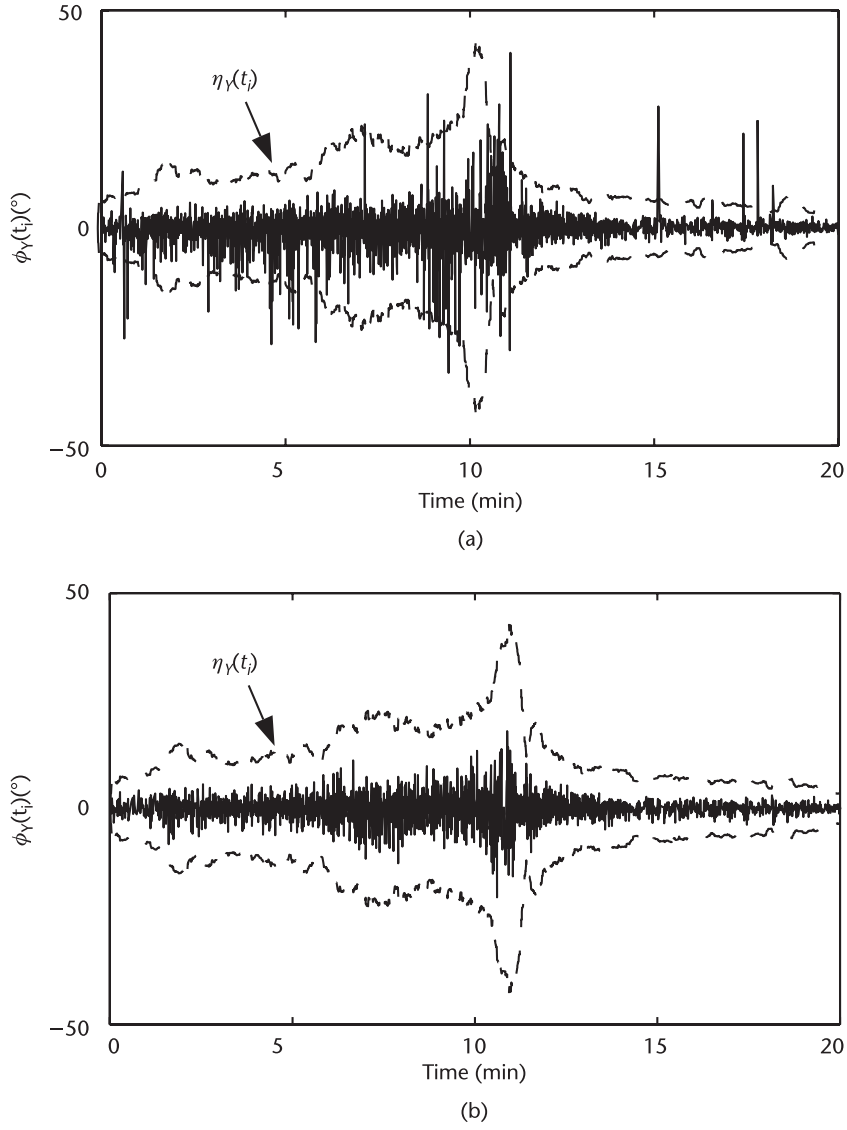

Figure 8.11 The EDR signal $\phi_Y(t_i)$ estimated (a) before and (b) after outlier correction/rejection. Dashed lines denote the running threshold $\eta_Y(t_i)$. The parameter values used are $N_e = 50$ and $C = 5$.

Although the QRS-VCG loop alignment EDR algorithm is developed for recordings with three orthogonal leads, it can still be applied when only two orthogonal leads are available. In this case the rotation matrix $\mathbf{Q}$ would be 2×2 and represent rotation around the lead orthogonal to the plane defined by the two leads.

Another approach to estimate the rotation angles of the electrical axis is by means of its intrinsic components, determined from the last 30 ms of the QR segment for each loop [10]. Using a similar idea, principal component analysis is applied to measurements of gravity center and inertial axes of each loop [23]; for each beat a QRS loop is constructed comprising 120 ms around the R peak and its center of gravity is computed yielding three coordinates referred to the axes of the reference system; the inertial axes in the space are also obtained and characterized by the

three angles that each inertial axis forms with the axes of reference; finally, the first principal component of the set of the computed parameters is identified as the respiratory activity.

8.3 EDR Algorithms Based on HR Information

Certain methods exploit the HRV spectrum to derive respiratory information. The underlying idea is that the component of the HR in the HF band (above 0.15 Hz) generally can be ascribed to the vagal respiratory sinus arrhythmia. Figure 8.12 displays the power spectrum of a HR signal during resting conditions and 90° head-up tilt, obtained by a seventh-order AR model. Although the power spectrum patterns depend on the particular interactions between the sympathetic and parasympathetic systems in resting and tilt conditions, two major components are detectable at low and high frequencies in both cases. The LF band (0.04 to 0.15 Hz) is related to short-term regulation of blood pressure whereas the extended HF band (0.15 Hz to half the mean HR expressed in Hz) reflects respiratory influence on HR.

Most EDR algorithms based on HR information estimate the respiratory activity as the HF component in the HRV signal and, therefore, the HRV signal itself can be used as an EDR signal. The HRV signal can be filtered (e.g., from 0.15 Hz to half the mean HR expressed in Hz, which is the highest meaningful frequency since the intrinsic sampling frequency of the HRV signal is given by the HR) to reduce HRV components unrelated to respiration.

The HRV signal is based on the series of beat occurrence times obtained by a QRS detector. A preprocessing step is needed in which QRS complexes are detected and clustered, since only beats from sinus rhythm (i.e., originated from the sinoatrial node) should be analyzed. Several definitions of signals for representing HRV have been suggested, for example, based on the interval tachogram, the interval function, the event series, or the heart timing signal; see [36] for further details on different HRV signal representations.

The presence of ectopic beats, as well as missed or falsely detected beats, results in fictitious frequency components in the HRV signal which must be avoided.

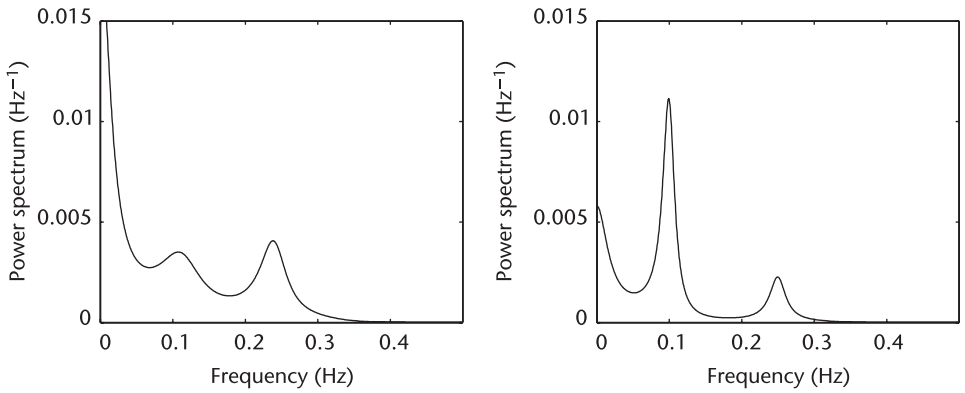

Figure 8.12 Power spectrum of a HR signal during resting conditions (left) and 90° head-up tilt (right).

A method to derive the HRV signal in the presence of ectopic beats based on the heart timing signal has been proposed [37].

8.4 EDR Algorithms Based on Both Beat Morphology and HR

Some methods derive respiratory information from the ECG by exploiting beat morphology and HR [22, 30]. A multichannel EDR signal can be constructed with EDR signals obtained both from the EDR algorithms based on beat morphology (Section 8.2) and from HR (Section 8.3). The power spectra of the EDR signals based on beat morphology can be crosscorrelated with the HR-based spectrum in order to reduce components unrelated to respiration [22].

A different approach is to use an adaptive filter which enhances the common component present in two input signals while attenuating uncorrelated noise. It was mentioned earlier that both ECG wave amplitudes and HR are influenced by respiration, which can be considered the common component. Therefore, the respiratory signal can be estimated by an adaptive filter applied to the series of RR intervals and R wave amplitudes [30]; see Figure 8.13(a). The series $a_r(i)$ denotes the R wave amplitude of the ith beat and is used as the reference input, whereas $rr(i)$ denotes the RR interval series and is the primary input. The filter output $r(i)$ is the estimate of the respiratory activity. The filter structure is not symmetric with respect to its inputs. The effectiveness of the two possible input configurations depends on the application [30]. This filter can be seen as a particular case of a more general adaptive filter whose reference input is the RR interval series $rr(i)$ and whose primary input is any of the EDR signals based on beat morphology, $e_j(i)$ $(j = 1, \ldots, J)$, or even a combination of them; see Figure 8.13(b). The interchange of reference and primary inputs could be also considered.

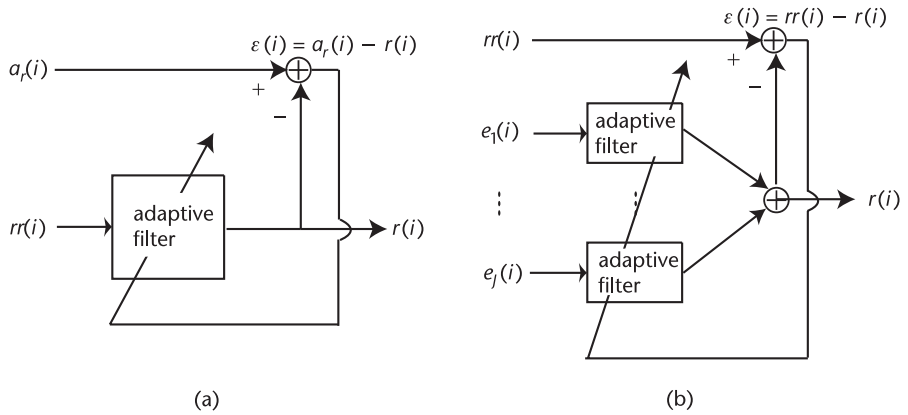

Figure 8.13 Adaptive estimation of respiratory signal. (a) The reference input is the R wave amplitude series $a_r(i)$, the primary input is the RR interval series $rr(i)$, and the filter output is the estimate of the respiratory signal $r(i)$. (b) The reference input is the RR interval series $rr(i)$ and the primary input is a combination of different EDR signals based on beat morphology $e_j(i)$, $j = 1, \ldots, J$, J denotes the number of EDR signals; the filter output is the estimate of the respiratory signal $r(i)$.

8.5 Estimation of the Respiratory Frequency

In this section the estimation of the respiratory frequency from the EDR signal, obtained by any of the methods previously described in Sections 8.2, 8.3, and 8.4, is presented. It may comprise spectral analysis of the EDR signal and estimation of the respiratory frequency from the EDR spectrum.

Let us define a multichannel EDR signal $e_j(t_i)$, where $j = 1, \ldots, J, i = 1, \ldots, L$, J denotes the number of EDR signals, and L the number of samples of the EDR signals. For single-lead EDR algorithms based on wave amplitudes (Section 8.2.1) and for EDR algorithms based on HR (Section 8.3), $J = 1$. For EDR algorithms based on multilead QRS area (Section 8.2.2) or on QRS-VCG loop alignment (Section 8.2.3), the value of J depends on the number of available leads. The value of J for EDR algorithms based on both beat morphology and HR depends on the particular choice of method.

Each EDR signal can be unevenly sampled, $e_j(t_i)$, as before, or evenly sampled, $e_j(n)$, coming either from interpolating and resampling of $e_j(t_i)$ or from an EDR signal which is intrinsically evenly sampled. The EDR signals coming from any source related to beats could be evenly sampled if represented as a function of beat order or unevenly sampled if represented as function of beat occurrence time t_i, but which could become evenly sampled when interpolated. An EDR signal based on direct filtering of the ECG is evenly sampled.

The spectral analysis of an evenly sampled EDR signal can be performed using either nonparametric methods based on the Fourier transform or parametric methods such as AR modeling. An unevenly sampled EDR signal may be interpolated and resampled at evenly spaced times, and then processed with the same methods as for an evenly sampled EDR signal. Alternatively, an unevenly sampled signal may be analyzed by spectral techniques designed to directly handle unevenly sampled signals such as Lomb's method [38].

8.5.1 Nonparametric Approach

In the nonparametric approach, the respiratory frequency is estimated from the location of the largest peak in the respiratory frequency band of the power spectrum of the multichannel EDR signal, using the Fourier transform if the signal is evenly sampled or Lomb's method if the signal is unevenly sampled.

In order to handle nonstationary EDR signals with a time-varying respiratory frequency, the power spectrum is estimated on running intervals of T_s seconds, where the EDR signal is assumed to be stationary. Individual running power spectra of each EDR signal $e_j(t_i)$ are averaged in order to reduce their variance. For the jth EDR signal and kth running interval of T_s- second length, the power spectrum $S_{j,k}(f)$ results from averaging the power spectra obtained from subintervals of length T_m seconds ($T_m < T_s$) using an overlap of $T_m/2$ seconds. A T_s-second spectrum is estimated every t_s seconds. The variance of $S_{j,k}(f)$ is further reduced by "peak-conditioned" averaging in which selective averaging is performed only on those $S_{j,k}(f)$ which are sufficiently peaked. Here, "peaked" means that a certain percentage (ξ) of the spectral power must be contained in an interval centered

around the largest peak $f_p(j,k)$, otherwise the spectrum is omitted from averaging. In mathematical terms, peak-conditioned averaging is defined by

$$\overline{S}_k(f) = \sum_{l=0}^{L_s-1} \sum_{j=1}^{J} \chi_{j,k-l} S_{j,k-l}(f), \quad k = 1, 2, \ldots \tag{8.12}$$

where the parameter L_s denotes the number of T_s-second intervals used for computing the averaged spectrum $\overline{S}_k(f)$. The binary variable $\chi_{j,k}$ indicates if the spectrum $S_{j,k}(f)$ is peaked or not, defined by

$$\chi_{j,k} = \begin{cases} 1 & P_{j,k} \geq \xi \\ 0 & \text{otherwise} \end{cases} \tag{8.13}$$

where the relative spectral power $P_{j,k}$ is given by

$$P_{j,k} = \frac{\displaystyle\int_{(1-\mu)\, f_p(j,k)}^{(1+\mu)\, f_p(j,k)} S_{j,k}(f)df}{\displaystyle\int_{0.1}^{f_{max}(k)} S_{j,k}(f)df} \tag{8.14}$$

where the value of $f_{max}(k)$ is given by half the mean HR expressed in Hz in the kth interval and μ determines the width of integration interval.

Figure 8.14 illustrates the estimation of the power spectrum $S_{j,k}(f)$ using different values of T_m. It can be appreciated that larger values of T_m yield spectra with better resolution and, therefore, more accurate estimation of the respiratory frequency. However, the respiratory frequency does not always correspond to a unimodal peak (i.e., showing a single frequency peak), but to a bimodal peak,

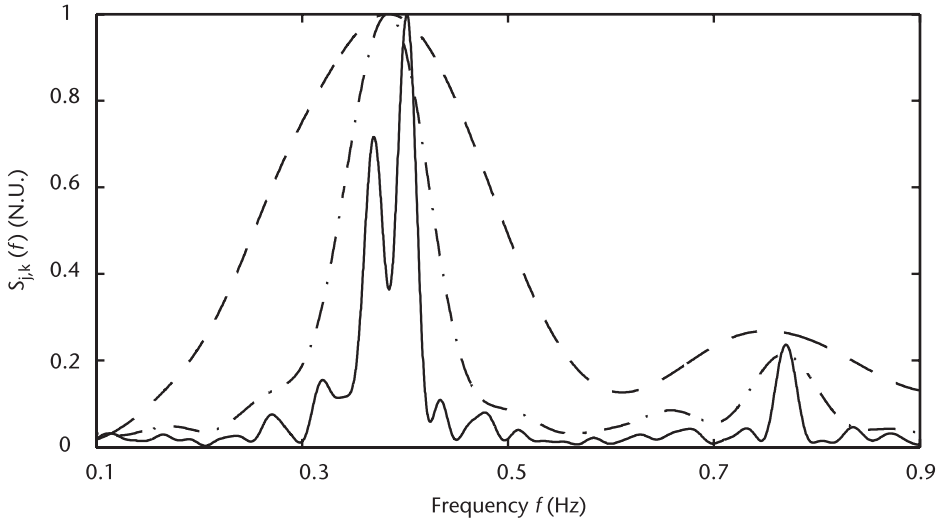

Figure 8.14 The power spectrum $S_{j,k}(f)$ computed for $T_m = 4$ seconds (dashed line), 12 seconds (dashed/dotted line), and 40 seconds (solid line), using $T_s = 40$ seconds.

sometimes observed in ECGs recorded during exercise. In such situations, smaller values of T_m should be used to estimate the gross dominant frequency.

Estimation of the respiratory frequency $\hat{f}_r(k)$ as the largest peak of $\overline{S}_k(f)$ comes with the risk of choosing the location of a spurious peak. This risk is, however, considerably reduced by narrowing down the search interval to only include frequencies in an interval of $2\delta_f$ Hz centered around a reference frequency $f_w(k)$: $[f_w(k) - \delta_f, f_w(k) + \delta_f]$. The reference frequency is obtained as an exponential average of previous estimates, using

$$f_w(k+1) = \beta f_w(k) + (1-\beta)\hat{f}_r(k) \tag{8.15}$$

where β denotes the forgetting factor. The procedure to estimate the respiratory frequency is summarized in Figure 8.15.

Respiratory frequency during a stress test has been estimated using this procedure in combination with both the multilead QRS area and the QRS-VCG loop alignment EDR algorithms, described in Sections 8.2.2 and 8.2.3, respectively [28]. Results are compared with the respiratory frequency obtained from simultaneous airflow respiratory signals. An estimation error of 0.022±0.016 Hz (5.9±4.0%) is achieved by the QRS-VCG loop alignment EDR algorithm and of 0.076±0.087 Hz (18.8±21.7%) by the multilead QRS area EDR algorithm. Figure 8.16 displays an example of the respiratory frequency estimated from the respiratory signal and from the ECG using the QRS-VCG loop alignment EDR algorithm. Lead X of the observed and reference loop are displayed at different time instants during the stress test.

8.5.2 Parametric Approach

Parametric AR model-based methods have been used to estimate the respiratory frequency in stationary [29] and nonstationary situations [27, 39]. Such methods offer automatic decomposition of the spectral components and, consequently, estimation of the respiratory frequency. Each EDR signal $e_j(n)$ can be seen as the output of an AR model of order P,

$$e_j(n) = -a_{j,1}e_j(n-1) - \cdots - a_{j,P}e_j(n-P) + v(n) \tag{8.16}$$

where n indexes the evenly sampled EDR signal, $a_{j,1}, \ldots, a_{j,P}$ are the AR parameters, and $v(n)$ is white noise with zero mean and variance σ^2. The model transfer function is

$$H_j(z) = \frac{1}{A_j(z)} = \frac{1}{\sum_{l=0}^{P} a_{j,l}z^{-l}} = \frac{1}{\prod_{p=1}^{P}(1 - z_{j,p}z^{-1})} \tag{8.17}$$

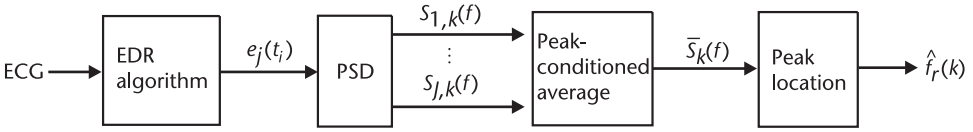

Figure 8.15 Block diagram of the estimation of respiratory frequency. PSD: power spectral density.

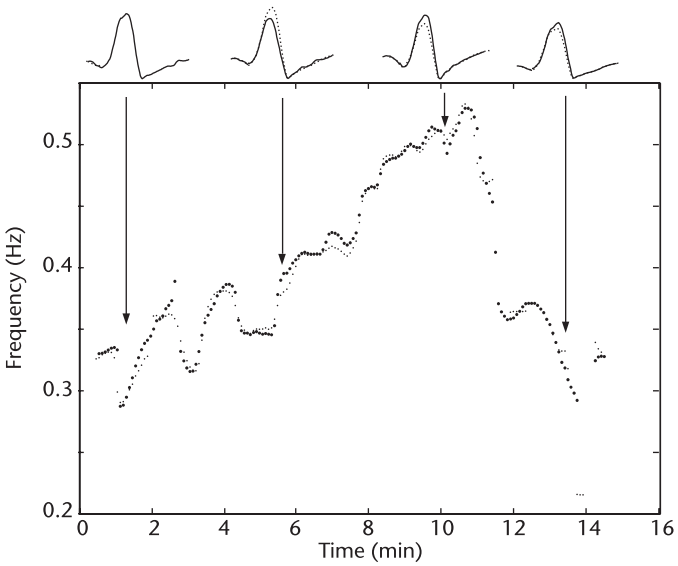

Figure 8.16 The respiratory frequency estimated from the respiratory signal (f_r, small dots) and from the ECG ($\hat{f}_r$, big dots) during a stress test using QRS-VCG loop alignment EDR algorithm. Lead X of the observed (solid line) and reference (dotted line) loop are displayed above the figure at different time instants. Parameter values: $T_s = 40$ seconds, $t_s = 5$ seconds, $T_m = 12$ seconds, $L_s = 5$, $\mu = 0.5$, $\xi = 0.35$, $\beta = 0.7$, $\delta_f = 0.2$ Hz, and $f_w(1) = \arg\max_{0.15 \le f \le 0.4} (\overline{S}_1(f))$.

where $a_{j,0} = 1$ and the poles $z_{j,p}$ appear in complex-conjugate pairs since the EDR signal is real. The corresponding AR spectrum can be obtained by evaluating the following expression for $z = e^{j\omega}$,

$$S_j(z) = \frac{\sigma^2}{A_j(z)\,A_j(z^{-1})} = \frac{\sigma^2}{\prod_{p=1}^{P}(1 - z_{j,p}z^{-1})(1 - z_{j,p}^{*}z)} \tag{8.18}$$

It can be seen from (8.18) that the roots of the polynomial $A_j(z)$ and the spectral peaks are related. A simple way to estimate peak frequencies is by the phase angle of the poles $z_{j,p}$,

$$\hat{f}_{j,p} = \frac{1}{2\pi} \arctan\left(\frac{\Im(z_{j,p})}{\Re(z_{j,p})}\right) \cdot f_s \tag{8.19}$$

where f_s is the sampling frequency of $e_j(n)$. A detailed description on peak frequency estimation from AR spectrum can be found in [36]. The selection of the respiratory frequency $\hat{f}_r$ from the peak frequency estimates $\hat{f}_{j,p}$ depends on the chosen EDR signal and the AR model order P. An AR model of order 12 has been fitted to a HRV signal and the respiratory frequency estimated as the peak frequency estimate with the highest power lying in the expected frequency range [27]. Another approach has been to determine the AR model order by means of the Akaike criterion and then to select the central frequency of the HF band as the respiratory frequency [29]. Results have been compared to those extracted from simultaneous strain gauge respiratory signal and a mean error of 0.41 ± 0.48 breaths per minute (0.007 ± 0.008 Hz) has been reported.

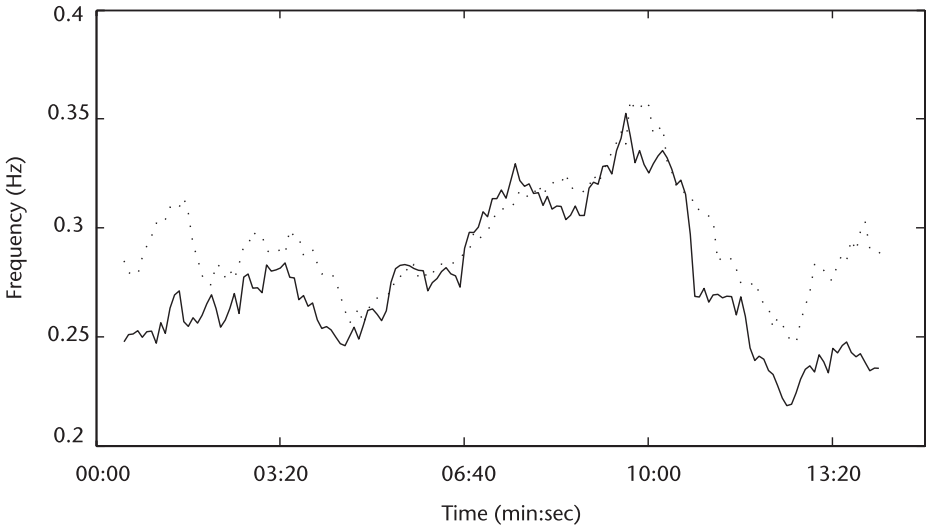

Figure 8.17 Respiratory frequency during a stress test, estimated from the respiratory signal (f_r, dotted) and from the HRV signal ($\hat{f}_r$, solid) using seventh-order AR modeling. The parameter values used are: $P = 7$, $T_s = 60$ seconds, and $t_s = 5$ seconds.

Figure 8.17 displays an example of the respiratory frequency during a stress test, estimated both from an airflow signal and from the ECG using parametric AR modeling. The nonstationarity nature of the signals during a stress test is handled by estimating the AR parameters on running intervals of T_s seconds, shifted by t_s seconds, where the EDR signal is supposed to be stationary, as in the nonparametric approach of Section 8.5.1. The EDR signal in this case is made to be the HRV signal which has been filtered in each interval of T_s second duration using a FIR filter with passband from 0.15 Hz to the minimum between 0.9 Hz (respiratory frequency is not supposed to exceed 0.9 Hz even in the peak of exercise) and half the mean HR expressed in Hz in the corresponding interval. The AR model order has been set to $P = 7$, as in Figure 8.12. The peak frequency estimate $\hat{f}_{j,p}$ with the highest power is selected as the respiratory frequency $\hat{f}_r$ in each interval.

The parametric approach can be applied to the multichannel EDR signal in a way similar to the nonparametric approach of Section 8.5.1. Selective averaging can be applied to the AR spectra $S_j(z)$ of each EDR signal $e_j(n)$, and the respiratory frequency can be estimated from the averaged spectrum in a restricted frequency interval. Another approach is the use of multivariate AR modeling [9] in which the cross-spectra of the different EDR signals are exploited for identification of the respiratory frequency.

8.5.3 Signal Modeling Approach

In Sections 8.5.1 and 8.5.2, nonparametric and parametric approaches have been applied to estimate the respiratory frequency from the power spectrum of the EDR signal. In this section, a different approach based on signal modeling is considered for identifying and quantifying the spectral component related to respiration.

The evenly sampled EDR signal $e_j(n)$ is assumed to be the sum of K complex undamped exponentials, according to the model

$$e_j(n) = \sum_{k=1}^{K} h_k e^{J\omega_k n} \tag{8.20}$$

where h_k denotes the amplitude and ω_k denotes the angular frequency. Since $e_j(n)$ is a real-valued signal, it is necessary that the complex exponentials in (8.20) occur in complex-conjugate pairs (i.e., K must be even). The problem of interest is to determine the frequencies of the exponentials given the observations $e_j(n)$, and to identify the respiratory frequency, f_r.

A direct approach would be to set up a nonlinear LS minimization problem in which the signal parameters h_k and ω_k would be chosen so as to minimize

$$\left\| e_j(n) - \sum_{k=1}^{K} h_k e^{J\omega_k n} \right\|_F^2 \tag{8.21}$$

However, since nonlinear minimization is computationally intensive and cumbersome, indirect approaches are often used. These are based on the fact that, in the absence of noise and for the model in (8.20), $e_j(n)$ is exactly predictable as a linear combination of its K past samples,

$$e_j(n) = -a_{j,1}e_j(n-1) - \cdots - a_{j,K}e_j(n-K), \quad n = K, \ldots, 2K-1 \tag{8.22}$$

which can be seen as an AR model of order K.

One such approach is due to Prony [40], developed to estimate the parameters of a sum of complex damped exponentials. Our problem can be seen as a particular case in which the damping factors are zero; further details on the derivation of Prony's method for undamped exponentials are found in [9].

A major drawback of Prony-based methods is the requirement of a priori knowledge of the model order K (i.e., the number of complex exponentials). When it is unknown, it must be estimated from the observed signal, for example, using techniques similar to AR model order estimation.

Another approach to estimate the frequencies of a sum of complex exponentials is by means of state space methods [41]. The EDR signal $e_j(n)$ is assumed to be generated by the following state space model:

$$\begin{aligned} \mathbf{e}_j(n+1) &= \mathbf{F}\mathbf{e}_j(n) \\ e_j(n) &= \mathbf{h}^T\mathbf{e}_j(n) \end{aligned} \tag{8.23}$$

where

$$\mathbf{e}_j(n) = \begin{bmatrix} e_j(n-1) \\ e_j(n-2) \\ \vdots \\ e_j(n-K) \end{bmatrix}, \quad \mathbf{F} = \begin{bmatrix} a_1 & a_2 & \ldots & a_{K-1} & a_K \\ 1 & 0 & \ldots & 0 & 0 \\ 0 & 1 & \ldots & 0 & 0 \\ \vdots & \vdots & & \vdots & \\ 0 & 0 & \ldots & 1 & 0 \end{bmatrix}, \quad \mathbf{h} = \begin{bmatrix} a_1 \\ a_2 \\ \ldots \\ a_K \end{bmatrix} \tag{8.24}$$

It can be shown that the eigenvalues of the $K \times K$ matrix $\mathbf{F}$ are equal to $e^{j\omega_k}$, $k = 1, \ldots, K$, and thus the frequencies can be obtained once $\mathbf{F}$ is estimated from data [41]. Then, respiratory frequency has to be identified from the frequency estimates.

Such an approach has been applied to HR series to estimate the respiratory frequency, considered as the third lowest frequency estimate [25]. Respiratory frequency estimated is compared to that extracted from simultaneous respiratory recordings. A mean absolute error lower than 0.03 Hz is reported during rest and tilt-test. However, the method fails to track the respiratory frequency during exercise due to the very low SNR.

8.6 Evaluation

In order to evaluate the performance of EDR algorithms, the derived respiratory information should be compared to the respiratory information simultaneously recorded. However, simultaneous recording of ECG and respiratory signals is difficult to perform in certain situations, such as sleep studies, ambulatory monitoring, and stress testing. In such situations, an interesting alternative is the design of a simulation study where all signal parameters can be controlled.

A dynamical model for generating simulated ECGs has been presented [42]. The model generates a trajectory in a three-dimensional state space with coordinates (x,y,z), which moves around an attracting limit cycle of unit radius in the (x,y) plane; each cycle corresponds to one RR interval. The ECG waves are generated by attractors/repellors in the z direction. Baseline wander is introduced by coupling the baseline value in the z direction to the respiratory frequency. The z variable of the three-dimensional trajectory yields a simulated ECG with realistic PQRST morphology. The HRV is incorporated in the model by varying the angular velocity of the trajectory as it moves around the limit cycle according to variations in the length of RR intervals. A bimodal power spectrum consisting of the sum of two Gaussian distributions is generated to simulate a peak in the LF band, related to short-term regulation of blood pressure, and another peak in the HF band, related to respiratory sinus arrhythmia. An RR interval series with the former power spectrum is generated and the angular velocity of the trajectory around the limit cycle is defined from it. Time-varying power spectra can be used to simulate respiratory signals with varying frequency. Observational uncertainty is incorporated by adding zero-mean Gaussian noise. Simulated ECGs generated by this model can be used to evaluate EDR algorithms based on HR information (Section 8.3) and single-lead EDR algorithms based on the modulation of wave amplitudes (Section 8.2.1). However, it is not useful to evaluate multilead EDR algorithms based on estimating the rotation of the heart's electrical axis.

A simulation study to evaluate multilead EDR algorithms based on beat morphology (Sections 8.2.2 and 8.2.3) on exercise ECGs has been presented [28]. The study consists of a set of computer-generated reference exercise ECGs to which noise and respiratory influence have been added.

First, a noise-free 12-lead ECG is simulated from a set of 15 beats (templates) extracted from rest, exercise, and recovery of a stress test using weighted averaging. The HR and ST depression of each template is modified to follow a predefined ST/HR pattern. The simulated signals result from concatenation of templates such that HR and ST depression evolve linearly with time. Then, the VCG signal is synthesized from the simulated 12-lead ECG.

In order to account for respiratory influence, the simulated VCG is transformed on a sample-by-sample basis with a three-dimensional rotation matrix defined by time-varying angles. The angular variation around each axis is modeled by the product of two sigmoidal functions reflecting inhalation and exhalation [43], such that for lead X,

$$\phi_X(n) = \sum_{p=0}^{\infty} \zeta_X \frac{1}{1+e^{-\lambda_i(p)(n-\kappa_i(p))}} \frac{1}{1+e^{\lambda_e(p)(n-\kappa_e(p))}} \tag{8.25}$$

$$\lambda_i(p) = 20\frac{f_r(p)}{f_s}, \kappa_i(p) = \kappa_i(p-1) + \frac{f_s}{f_r(p-1)}, \kappa_i(0) = 0.35\, f_s,$$

$$\lambda_e(p) = 15\frac{f_r(p)}{f_s}, \kappa_e(p) = \kappa_e(p-1) + \frac{f_s}{f_r(p-1)}, \kappa_e(0) = 0.6\, f_s$$

where n denotes sample index, p denotes each respiratory cycle index, $\frac{1}{\lambda_i(p)}$ and $\frac{1}{\lambda_e(p)}$ are the duration of inhalation and exhalation, respectively, $\kappa_i(p)$ and $\kappa_e(p)$ are the time delays of the sigmoidal functions, f_s is the sampling rate, $f_r(p)$ is the respiratory frequency, and ζ_X is the maximum angular variation around lead X, which has been set to 5°. The same procedure is applied to leads Y and Z, with $\zeta_Y = \zeta_Z = \zeta_X$. To account for the dynamic nature of the respiratory frequency during a stress test, the simulated respiratory frequency $f_r(p)$ follows a pattern varying from 0.2 to 0.7 Hz, see Figure 8.18. A similar respiratory pattern has been observed in several actual stress tests.

Finally, noise is added to the concatenated ECG signals, obtained as the residual between raw exercise ECGs and a running average of the heartbeats [1]. The noise contribution to the VCG is synthesized from the 12-lead noise records. In Figure 8.19 lead X of a simulated VCG is displayed during different stages of a stress test. The simulation procedure is summarized in Figure 8.20.

This simulation study has been used to evaluate the performance of the methods based on the multilead QRS area and the QRS-VCG loop alignment in estimating the respiratory frequency from the ECG [28]. An estimation error of 0.002±0.001 Hz (0.5±0.2%) is achieved by QRS-VCG loop alignment while an error of 0.005±0.004 Hz (1.0±0.7%) is achieved by multilead QRS area. The mean and the standard deviation of the estimated respiratory frequency by both approaches are displayed in Figure 8.21.

This simulation study is not useful for evaluating EDR algorithms based on HR information (Section 8.3) since respiratory influence only affects beat morphology but not beat occurrence time. However, it can be easily upgraded to include respiration effect on HR. For example, HR trends can be generated by an AR model like those in Figure 8.12 whose HF peak is driven by respiratory frequency.

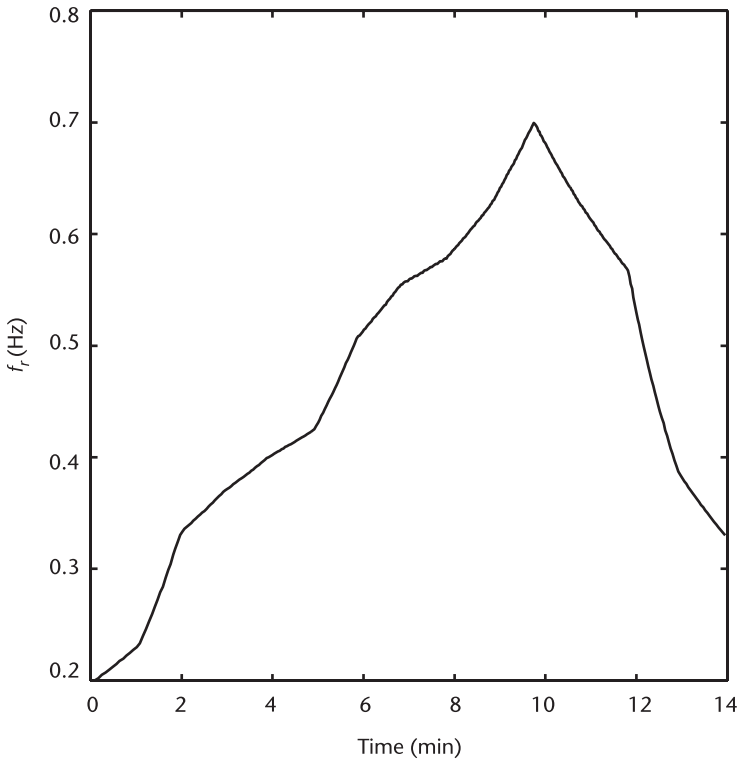

Figure 8.18 Simulated respiratory frequency pattern.

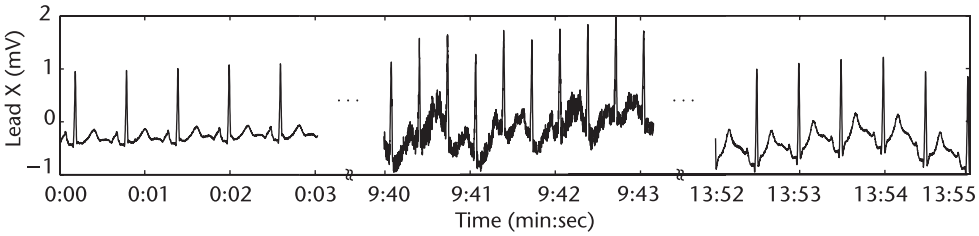

Figure 8.19 Simulated ECG signal at onset, peak exercise, and end of a stress test.

The above simulation designs can be seen as particular cases of a generalized simulation used to evaluate EDR algorithms based on beat morphology (single- or multilead) and EDR algorithms based on HR. First, beat templates are generated, either from a model [42] or from real ECGs [28]. The simulated ECG signals result from concatenation of beat templates following RR interval series with power spectrum such that the HF peak is driven by respiratory frequency. Long-term variations of QRS morphology unrelated to respiration and due to physiological conditions such as ischemia can be added to the simulated ECG signals. The respiratory influence on beat morphology is introduced by simulating the rotation of the heart's electrical axis induced by respiration. Finally, noise is generated either from a model [42] or from real ECGs [28] and added to the simulated ECGs. The generalized simulation design is summarized in Figure 8.22.

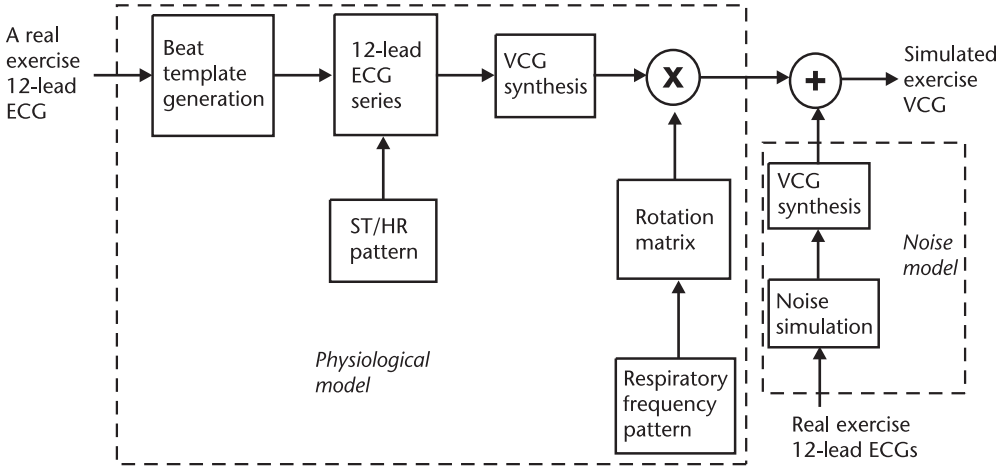

Figure 8.20 Block diagram of the simulation design. Note that the 12-lead ECGs used for signal and noise generation are different.

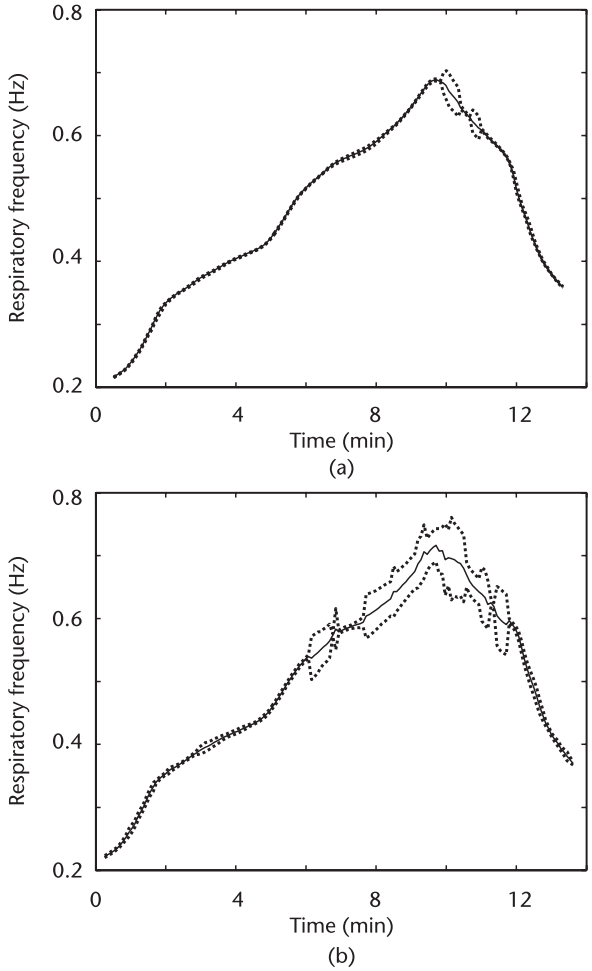

Figure 8.21 The mean respiratory frequency (solid line) ± the SD (dotted line) estimated in the simulation study using (a) QRS-VCG loop alignment and (b) multilead QRS area approaches.

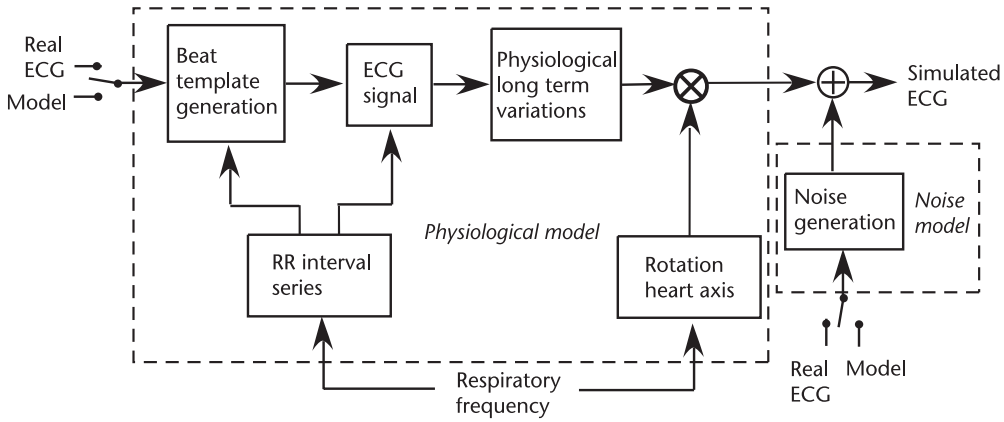

Figure 8.22 Block diagram of the generalized simulation design. Note that the ECGs used for signal and noise generation are different.

8.7 Conclusions

In this chapter, several EDR algorithms have been presented which estimate a respiratory signal from the ECG. They have been divided into three categories:

1. EDR algorithms based on beat morphology, namely, those based on ECG wave amplitude, on multilead QRS area, and on QRS-VCG loop alignment (Section 8.2);
2. EDR algorithms based on HR information (Section 8.3);
3. EDR algorithms based on both beat morphology and HR (Section 8.4).

The choice of a particular EDR algorithm depends on the application. In general, EDR algorithms based on beat morphology are more accurate than EDR algorithms based on HR information, since the modulation of HRV by respiration is sometimes lost or embedded in other parasympathetic interactions.

Amplitude EDR algorithms have been reported to perform satisfactorily when only single-lead ECGs are available, as is usually the case in sleep apnea monitoring [14, 17, 18, 20, 21, 32]. When multilead ECGs are available, EDR algorithms based on either multilead QRS area or QRS-VCG loop alignment are preferable. The reason is that due to thorax anisotropy and its intersubject variability together with the intersubject electrical axis variability, respiration influences ECG leads in different ways; the direction of the electrical axis, containing multilead information, is likely to better reflect the effect of respiration than wave amplitudes of a single lead. In stationary situations, both multilead QRS area or QRS-VCG loop alignment EDR algorithms estimate a reliable respiratory signal from the ECG [5, 22]. However, in nonstationary situations, such as in stress testing, the QRS-VCG loop alignment approach is preferred over the multilead QRS area [28]. Electrocardiogram-derived respiration algorithms based on both beat morphology and HR may be appropriate when only a single-lead ECG is available and the respiration effect on that lead is not pronounced [30]. The power spectra of the EDR signals based on morphology and HR can be cross-correlated to reduce spurious

peaks and enhance the respiratory frequency. However, the likelihood of having an EDR signal with pronounced respiration modulation is better when the signal is derived from multilead ECGs; cross-correlation with the HR power spectrum may in those situations worsen the results due to poor respiratory HR modulation [22].

There are still certain topics in the EDR field which deserve further study. One is the robustness of the EDR algorithms in different physiological conditions. In this chapter, robustness to long-term QRS morphologic variations due to, for example, ischemia, has been addressed. The study of nonunimodal respiratory patterns should be considered when estimating the respiratory frequency from the ECG by techniques like, for example, spectral coherence. Finally, one of the motivations and future challenges in the EDR field is the study of the cardio-respiratory coupling and its potential value in the evaluation of the autonomic nervous system activity.

References

[1] Bailón, R., et al., "Coronary Artery Disease Diagnosis Based on Exercise Electrocardiogram Indexes from Repolarisation, Depolarisation and Heart Rate Variability," *Med. Biol. Eng. Comput.*, Vol. 41, 2003, pp. 561–571.

[2] Einthoven, W., G. Fahr, and A. Waart, "On the Direction and Manifest Size of the Variations of Potential in the Human Heart and on the Influence of the Position of the Heart on the Form of the Electrocardiogram," *Am. Heart J.*, Vol. 40, 1950, pp. 163–193.

[3] Flaherty, J., et al., "Influence of Respiration on Recording Cardiac Potentials," *Am. J. Cardiol.*, Vol. 20, 1967, pp. 21–28.

[4] Riekkinen, H., and P., Rautaharju, "Body Position, Electrode Level and Respiration Effects on the Frank Lead Electrocardiogram," *Circ.*, Vol. 53, 1976, pp. 40–45.

[5] Moody, G., et al., "Derivation of Respiratory Signals from Multi-Lead ECGs," *Proc. Computers in Cardiology*, IEEE Computer Society Press, 1986, pp. 113–116.

[6] Grossman, P., and K. Wientjes, "Respiratory Sinus Arrhythmia and Parasympathetic Cardiac Control: Some Basic Issues Concerning Quantification, Applications and Implications," in P. Grossman, K. Janssen, and D. Vaitl, (eds.), *Cardiorespiratory and Cardiosomatic Psychophysiology*, New York: Plenum Press, 1986, pp. 117–138.

[7] Zhang, P., et al., "Respiration Response Curve Analysis of Heart Rate Variability," *IEEE Trans. Biomed. Eng.*, Vol. 44, 1997, pp. 321–325.

[8] Pallás-Areni, R., J. Colominas-Balagué, and F. Rosell, "The Effect of Respiration-Induced Heart Movements on the ECG," *IEEE Trans. Biomed. Eng.*, Vol. 36, No. 6, 1989, pp. 585–590.

[9] Marple, S., *Digital Spectral Analysis with Applications*, Englewood Cliffs, NJ: Prentice-Hall, 1996.

[10] Wang, R., and T. Calvert, "A Model to Estimate Respiration from Vectorcardiogram Measurements," *Ann. Biomed. Eng.*, Vol. 2, 1974, pp. 47–57.

[11] Pinciroli, F., R. Rossi, and L. Vergani, "Detection of Electrical Axis Variation for the Extraction of Respiratory Information," *Proc. Computers in Cardiology*, IEEE Computer Society Press, 1986, pp. 499–502.

[12] Zhao, L., S. Reisman, and T. Findley, "Derivation of Respiration from Electrocardiogram During Heart Rate Variability Studies," *Proc. Computers in Cardiology*, IEEE Computer Society Press, 1994, pp. 53–56.

[13] Caggiano, D., and S. Reisman, "Respiration Derived from the Electrocardiogram: A Quantitative Comparison of Three Different Methods," *Proc. of the IEEE 22nd Ann. Northeast Bioengineering Conf.*, IEEE Press, 1996, pp. 103–104.

[14] Dobrev, D., and I. Daskalov, "Two-Electrode Telemetric Instrument for Infant Heart Rate and Apnea Monitoring," *Med. Eng. Phys.*, Vol. 20, 1998, pp. 729–734.

[15] Travaglini, A., et al., "Respiratory Signal Derived from Eight-Lead ECG," *Proc. Computers in Cardiology*, Vol. 25, IEEE Press, 1998, pp. 65–68.

[16] Nazeran, H., et al., "Reconstruction of Respiratory Patterns from Electrocardiographic Signals," *Proc. 2nd Int. Conf. Bioelectromagnetism*, IEEE Press, 1998, pp. 183–184.

[17] Raymond, B., et al., "Screening for Obstructive Sleep Apnoea Based on the Electrocardiogram—The Computers in Cardiology Challenge," *Proc. Computers in Cardiology*, Vol. 27, IEEE Press, 2000, pp. 267–270.

[18] Mason, C., and L. Tarassenko, "Quantitative Assessment of Respiratory Derivation Algorithms," *Proc. 23rd Ann. IEEE EMBS Int. Conf.*, Istanbul, Turkey, 2001, pp. 1998–2001.

[19] Behbehani, K., et al., "An Investigation of the Mean Electrical Axis Angle and Respiration During Sleep," *Proc. 2nd Joint EMBS/BMES Conf.*, Houston, TX, 2002, pp. 1550–1551.

[20] Yi, W., and K. Park, "Derivation of Respiration from ECG Measured Without Subject's Awareness Using Wavelet Transform," *Proc. 2nd Joint EMBS/BMES Conf.*, Houston, TX, 2002, pp. 130–131.

[21] Chazal, P., et al., "Automated Processing of Single-Lead Electrocardiogram for the Detection of Obstructive Sleep Apnoea," *IEEE Trans. Biomed. Eng.*, Vol. 50, No. 6, 2003, pp. 686–696.

[22] Leanderson, S., P. Laguna, and L. Sörnmo, "Estimation of the Respiratory Frequency Using Spatial Information in the VCG," *Med. Eng. Phys.*, Vol. 25, 2003, pp. 501–507.

[23] Bianchi, A., et al., "Estimation of the Respiratory Activity from Orthogonal ECG Leads," *Proc. Computers in Cardiology*, Vol. 30, IEEE Press, 2003, pp. 85–88.

[24] Yoshimura, T., et al., "An ECG Electrode-Mounted Heart Rate, Respiratory Rhythm, Posture and Behavior Recording System," *Proc. 26th Ann. IEEE EMBS Int. Conf.*, Vol. 4, IEEE Press, 2004, pp. 2373–2374.

[25] Pilgram, B., and M. Renzo, "Estimating Respiratory Rate from Instantaneous Frequencies of Long Term Heart Rate Tracings," *Proc. Computers in Cardiology*, IEEE Computer Society Press, 1993, pp. 859–862.

[26] Varanini, M., et al., "Spectral Analysis of Cardiovascular Time Series by the S-Transform," *Proc. Computers in Cardiology*, Vol. 24, IEEE Press, 1997, pp. 383–386.

[27] Meste, O., G. Blain, and S. Bermon, "Analysis of the Respiratory and Cardiac Systems Coupling in Pyramidal Exercise Using a Time-Varying Model," *Proc. Computers in Cardiology*, Vol. 29, IEEE Press, 2002, pp. 429–432.

[28] Bailón, R., L. Sörnmo, and P. Laguna, "A Robust Method for ECG-Based Estimation of the Respiratory Frequency During Stress Testing," *IEEE Trans. Biomed. Eng.*, Vol. 53, No. 7, 2006, pp. 1273–1285.

[29] Thayer, J., et al., "Estimating Respiratory Frequency from Autoregressive Spectral Analysis of Heart Period," *IEEE Eng. Med. Biol.*, Vol. 21, No. 4, 2002, pp. 41–45.

[30] Varanini, M., et al., "Adaptive Filtering of ECG Signal for Deriving Respiratory Activity," *Proc. Computers in Cardiology*, IEEE Computer Society Press, 1990, pp. 621–624.

[31] Edenbrandt, L., and O. Pahlm, "Vectorcardiogram Synthesized from a 12-Lead ECG: Superiority of the Inverse Dower Matrix," *J. Electrocardiol.*, Vol. 21, No. 4, 1988, pp. 361–367.

[32] Mazzanti, B., C. Lamberti, and J. de Bie, "Validation of an ECG-Derived Respiration Monitoring Method," *Proc. Computers in Cardiology*, Vol. 30, IEEE Press, 2003, pp. 613–616.

[33] Pinciroli, F., et al., "Remarks and Experiments on the Construction of Respiratory Waveforms from Electrocardiographic Tracings," *Comput. Biomed. Res.*, Vol. 19, 1986, pp. 391–409.

[34] Sörnmo, L., "Vectorcardiographic Loop Alignment and Morphologic Beat-to-Beat Variability," *IEEE Trans. Biomed. Eng.*, Vol. 45, No. 12, 1998, pp. 1401–1413.

[35] Åström, M., et al., "Detection of Body Position Changes Using the Surface ECG," *Med. Biol. Eng. Comput.*, Vol. 41, No. 2, 2003, pp. 164–171.

[36] Sörnmo, L., and P. Laguna, *Bioelectrical Signal Processing in Cardiac and Neurological Applications*, Amsterdam: Elsevier (Academic Press), 2005.

[37] Mateo, J., and P. Laguna, "Analysis of Heart Rate Variability in the Presence of Ectopic Beats Using the Heart Timing Signal," *IEEE Trans. Biomed. Eng.*, Vol. 50, 2003, pp. 334–343.

[38] Lomb, N. R., "Least-Squares Frequency Analysis of Unequally Spaced Data," *Astrophys. Space Sci.*, Vol. 39, 1976, pp. 447–462.

[39] Mainardi, L., et al., "Pole-Tracking Algorithms for the Extraction of Time-Variant Heart Rate Variability Spectral Parameters," *IEEE Trans. Biomed. Eng.*, Vol. 42, No. 3, 1995, pp. 250–258.

[40] de Prony, G., "Essai expérimental et analytique: sur les lois de la dilatabilité de fluides élastiques et sur celles de la force expansive de la vapeur de l'eau et de la vapeur de l'alkool, à différentes températures," *J. E. Polytech.*, Vol. 1, No. 2, 1795, pp. 24–76.

[41] Rao, B., and K. Arun, "Model Based Processing of Signals: A State Space Approach," *Proc. IEEE*, Vol. 80, No. 2, 1992, pp. 283–306.

[42] McSharry, P., et al., "A Dynamical Model for Generating Synthetic Electrocardiogram Signals," *IEEE Trans. Biomed. Eng.*, Vol. 50, No. 3, 2003, pp. 289–294.

[43] Åström, M., et al., "Vectorcardiographic Loop Alignment and the Measurement of Morphologic Beat-to-Beat Variability in Noisy Signals," *IEEE Trans. Biomed. Eng.*, Vol. 47, No. 4, 2000, pp. 497–506.

[44] Dower, G., H. Machado, and J. Osborne, "On Deriving the Electrocardiogram from Vectorcardiographic Leads," *Clin. Cardiol.*, Vol. 3, 1980, pp. 87–95.

[45] Frank, E., "The Image Surface of a Homogeneous Torso," *Am. Heart J.*, Vol. 47, 1954, pp. 757–768.

Appendix 8A Vectorcardiogram Synthesis from the 12-Lead ECG

Although several methods have been proposed for synthesizing the VCG from the 12-lead ECG, the inverse transformation matrix of Dower is the most commonly used [31]. Dower et al. presented a method for deriving the 12-lead ECG from Frank lead VCG [44]. Each ECG lead is calculated as a weighted sum of the VCG leads X, Y, and Z using lead-specific coefficients based on the image surface data from the original torso studies by Frank [45]. The transformation operation used

to derive the eight independent leads (V1 to V6, I and II) of the 12-lead ECG from the VCG leads is given by

$$\mathbf{s}(n) = \mathbf{D}\mathbf{v}(n), \quad \mathbf{D} = \begin{bmatrix} -0.515 & 0.157 & -0.917 \\ 0.044 & 0.164 & -1.387 \\ 0.882 & 0.098 & -1.277 \\ 1.213 & 0.127 & -0.601 \\ 1.125 & 0.127 & -0.086 \\ 0.831 & 0.076 & 0.230 \\ 0.632 & -0.235 & 0.059 \\ 0.235 & 1.066 & -0.132 \end{bmatrix} \tag{8A.1}$$

where $\mathbf{s}(n)=[V_1(n)\ V_2(n)\ V_3(n)\ V_4(n)\ V_5(n)\ V_6(n)\ I(n)\ II(n)]^T$ and $\mathbf{v}(n)=[X(n)\ Y(n)\ Z(n)]^T$ contain the voltages of the corresponding leads, n denotes the sample index, and $\mathbf{D}$ is called the Dower transformation matrix. From (8A.1) it follows that the VCG leads can be synthesized from the 12-lead ECG by

$$\mathbf{v}(n) = \mathbf{T}\mathbf{s}(n) \tag{8A.2}$$

where $\mathbf{T} = (\mathbf{D}^T\mathbf{D})^{-1}\mathbf{D}^T$ is called the inverse Dower transformation matrix and given by

$$\mathbf{T} = \begin{bmatrix} -0.172 & -0.074 & 0.122 & 0.231 & 0.239 & 0.194 & 0.156 & -0.010 \\ 0.057 & -0.019 & -0.106 & -0.022 & 0.041 & 0.048 & -0.227 & 0.887 \\ -0.229 & -0.310 & -0.246 & -0.063 & 0.055 & 0.108 & 0.022 & 0.102 \end{bmatrix} \tag{8A.3}$$